August 27-31, 2023
FLORENCE - ITALY
ICWE 16
16th International Conference on Wind Engineering

Multi-unit gyroscopic stabilizer to control flutter of long-span bridges: sensitivity analysis

Gian Felice Giaccu [1], Luca Caracoglia [2]

[1]*Department of Architecture, Design and Urban Planning, University of Sassari, Palazzo del Pou Salit, Piazza Duomo 6, 07041 Alghero, Italy, gf.giaccu@uniss.it*
[2]*Department of Civil and Environmental Engineering, 400 Snell Engineering Ctr., Northeastern University, 360 Huntington Avenue, Boston, MA 02115, USA, lucac@coe.neu.edu*

SUMMARY:
Long-span, cable-supported bridges are sensitive to wind effects due to the deck slenderness and aerodynamic properties. Flutter is usually a major design concern. This study continues the investigation on a prototype of a gyroscopic device, used as an active stabilizer to improve flutter performance. A model of the gyroscopic device, installed at multiple sectional positions under the bridge deck, is used to assess effectiveness in increasing the critical flutter wind speed. The study evaluates the stabilizers' performance on a benchmark long-span bridge as a function of the gyricity. A parametric study is conducted to evaluate the stabilizer's performance on a benchmark long-span cable-supported bridge as a function of its mechanical properties. Critical speed has been calculated by varying the gyricity and the angular frequency of the gyroscope's dynamic system. The results demonstrate that a multi-unit gyroscopic stabilizer, within its practical operational range, can positively influence the bridge flutter threshold of the considered long-span bridge.
Keywords: long-span cable-supported bridges, flutter control, gyroscopic stabilizer.

1. INTRODUCTION

The last decade has witnessed significant evolutions in the design of long-span, cable-supported bridges. Longer spans necessitate the study of new methodologies to increase the performance of these structures against wind loads. Flutter instability occurs when a bridge is exposed to a wind speed above a certain critical threshold. Above this threshold, vertical and torsional deck vibrations couple together. The diverging deck vibration can yield catastrophic structural failure. Aeroelastic instability can be predicted by analyzing the deck aeroelastic coefficients or *Scanlan derivatives* (SDs) (Scanlan and Tomko, 1971). Various control methods have been proposed to improve the performance: aerodynamic countermeasures (Chen and Kareem, 2003; Kwon et al., 2000), control surfaces and appendages (Kwon and Chang, 2000; Kwon et al., 2000; Omenzetter et al., 2002), passive tuned-mass dampers (Chen and Kareem, 2003; Pourzeynali and Datta, 2003) and actively controlled devices (Kobayashi and Nagaoka, 1992; Wilde et al., 2001), among several others. Gyroscopic devices have routinely been employed in various engineering fields (D'Eleuterio, 1986; Ghommema et al., 2010; Kan et al., 1992) for vibration suppression but rarely considered in bridge engineering. A study has explored the application of gyroscopic devices for seismic vibration isolation (Carta et al., 2017) and recently considered their use as a stabilizer against bridge flutter (Giaccu and Caracoglia, 2021). This study continues the exploration of gyroscopic stabilizing devices to improve bridge flutter performance. Structural dynamic interaction between

the bridge deck and the gyroscopic devices is simulated by a reduced-order model. Multi-unit gyroscopic devices are installed at various sectional positions under the deck. Results suggest that the use of multi-unit gyroscopic stabilizers yields noteworthy increase of the critical wind speed, employing more devices with smaller mass moment of inertia compared to previous results using a larger, single unit stabilizer. The devices also exhibit robustness against variations of dynamic bridge properties.

2. MODEL DESCRIPTION

As a first example, two sets of gyroscopic devices are installed under the bridge deck at two deck cross sections, located at longitudinal deck coordinates $x_{\Omega,1}$ and $x_{\Omega,2}$. Fig. 1 shows the schematics of the stabilizer, installed underneath a truss-bridge deck superstructure at either cross section.

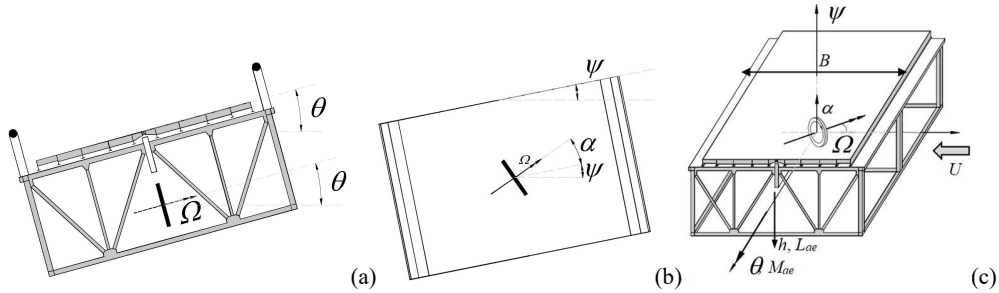

Figure 1. Bridge deck: (a) cross-section with gyroscopic stabilizer, (b) top view, (c) 3D lateral view with aeroelastic loads.

Each gyroscopic unit is modeled as a system with a lumped mass moment of inertia and three rotational DOFs (degrees of freedom), connected to the deck by a spring of stiffness k_α and a dashpot with damping coefficient c_α. Fig. 1 illustrates the layout of a single unit with the lumped rotating mass $M_{G,TOT}$; $J_{\Omega,p} = M_{G,TOT}\rho_\Omega^2$ is the polar mass moment of inertia with respect to the high-speed rotation axis; ρ_Ω is the radius of gyration of the gyroscopic stabilizer. The gyricity of the gyroscopic device can be expressed as $\mathbf{\Omega} = J_{\Omega,p}\boldsymbol{\omega}_G$ where $\boldsymbol{\omega}_G$ is the angular velocity vector of the gyroscope, which is usually pre-set. Each gyroscope has three DOFs, denoted as $\theta_1 = \theta(x_{\Omega,1},t), \psi_1(t), \alpha_1(t)$ and $\theta_2 = \theta(x_{\Omega,2},t), \psi_2(t), \alpha_2(t)$ (Fig. 1c), respectively for device "1", located at deck coordinate $x_{\Omega,1}$ and "2" at coordinate $x_{\Omega,2}$, with time t; $\theta(x,t)$ denotes the torsional rotation of the bridge deck at cross section x. This model is reduced to 1 DOF per stabilizer since $\psi_1 \approx \dot{\psi}_1 \approx \ddot{\psi}_1 \approx 0$ and $\psi_2 \approx \dot{\psi}_2 \approx \ddot{\psi}_2 \approx 0$ (Giaccu and Caracoglia, 2021); the dot marker indicates derivative with respect to time.

The bridge deck dynamic equilibrium equations (vertical direction and torsional rotation) at cross section x and time t are described in Eqs. (1-2) below, while Eqs. (3-4) are the lumped-mass gyroscope equilibria at $x_{\Omega,1}$ and $x_{\Omega,2}$:

$$m_h\partial_t^2 h + c_h\partial_t h + k_h h = L_{ae}(x,t) \tag{1}$$

$$[J_\theta + J_\alpha\delta(x-x_{\Omega1}) + J_\alpha\delta(x-x_{\Omega2})]\partial_t^2\theta + c_\theta\partial_t\theta + k_\theta\theta = -\Omega\delta(x-x_{\Omega1})\left(\dot{\psi}_1+\dot{\alpha}_1\right) - \Omega\delta(x-x_{\Omega2})\left(\dot{\psi}_2+\dot{\alpha}_2\right) + M_{ae}(x,t) \tag{2}$$

$$J_\alpha(\ddot{\psi}_1+\ddot{\alpha}_1) + c_\alpha\dot{\alpha}_1 + k_\alpha\alpha_1 = \Omega\dot{\theta}(x_{\Omega,1},t) \tag{3}$$

$$J_\alpha(\ddot{\psi}_2+\ddot{\alpha}_2) + c_\alpha\dot{\alpha}_2 + k_\alpha\alpha_2 = \Omega\dot{\theta}(x_{\Omega,2},t) \tag{4}$$

In the previous equations J_α, k_α and c_α respectively are moment of inertia, stiffness and damping coefficients of the lumped-mass gyroscopes, depending on the rotational DOFs α_1 and α_2. Aeroelastic lift and moment loads per unit deck span in Eqs. (1-2), $L_{ae}(x,t)$ and $M_{ae}(x,t)$, are described by SDs. Quantities J_θ and m_h are the inertial and mass terms of the deck; c_θ and c_h are equivalent viscous damping constants of the deck in the corresponding directions of vibration; k_θ and k_h simulate the elastic constants, related to the internal deck stiffness. The quantity $\delta(x)$ is the Dirac delta function. In Eqs. (3-4) $\dot{\theta}(x_{\Omega,1},t)$ and $\dot{\theta}(x_{\Omega,2},t)$ are angular (torsional) velocities of the deck at sections $x_{\Omega,1}$ and $x_{\Omega,2}$.

Eqs. (1-2) are first reduced to ordinary differential equations by modal superposition. In this study, modal superposition is limited to the two fundamental deck modes that mainly contribute to flutter, namely a fundamental flexural one ("$v1$") one and a torsional ("$t1$") one. Consequently, the deck displacements and rotations in Eqs. (1-2) are expressed as $h(x,t) \approx \xi_{v1}(t)Bh_{v1}(x)$, $\theta(x,t) \approx \xi_{t1}(t)\theta_{t1}(x)$ with: B deck width, $h_{v1}(x)$ and $\theta_{t1}(x)$ dimensionless deck mode shape functions, $\xi_{v1}(t)$ and $\xi_{t1}(t)$ generalized, dimensionless coordinates of modes $v1$ and $t1$.

Aeroelastic instability is solved by multi-mode approach (Jain, 1996). After modal expansion, a system of four generalized equations is derived in the dimensionless time $s = tU/B$. The variables of the reduced-order model are: ξ_g, $\xi_g' = \mathrm{d}\xi_g/\mathrm{d}s$ and $\xi_g'' = \mathrm{d}^2\xi_g/\mathrm{d}s^2$ with g={$v1$,$t1$}, and α_1, α_2. After Fourier transformation, incipient flutter instability is examined by enforcing simple harmonic deck motion; the generalized coordinates are expressed in vector form as $\bar{\boldsymbol{\xi}}_\Omega = \{\bar{\xi}_{v1}, \bar{\xi}_{t1}, \bar{\alpha}_1, \bar{\alpha}_2\}^T$, with superscript T denoting transpose operator and overbar Fourier transform. The vector $\bar{\boldsymbol{\xi}}_\Omega$ includes both the generalized coordinates of $v1$ and $t1$ and the relative gyroscope rotation variables. Flutter threshold is found after re-writing the equilibrium equations in the frequency domain and in homogenous form as $\mathbf{E}_\Omega(K,\chi)\bar{\boldsymbol{\xi}}_\Omega = \mathbf{0}$, where $\mathbf{E}_\Omega(K,\chi)$ is a complex matrix that depends on the SDs, the reduced frequency at flutter $K = \omega B/U$ and reduced angular frequency at flutter $\chi = \omega/\omega_{t1}$, normalized to the angular frequency of torsional mode t1, ω_{t1}.

3. NUMERICAL RESULTS

Numerical investigation is conducted on the full-scale structural model of the Golden Gate Bridge; structural model properties and SDs are derived from Jain (1996). The stabilizers, each having a rotating mass with a radius of 2 m and a thickness of 0.2 m, are installed at two cross sections under the deck, two units at ¼ span and two units at ¾ span (ℓ= deck span length) Results are presented in Fig. 2.

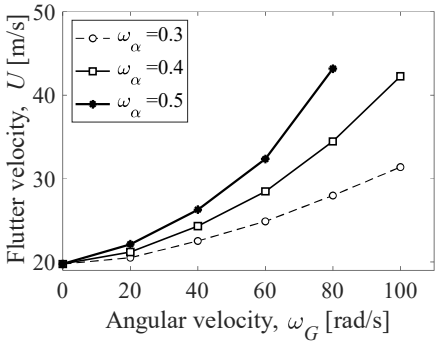

Figure 2. Flutter solution: sensitivity analysis results

In Fig. 2, the critical flutter speed has been calculated by varying the gyricity of each gyroscopic unit, Ω =kg m^2 rad s^{-1}, i.e., the angular velocity ω_G. The angular frequency of the gyroscope's dynamic system [Eq.(3) or (4)] is $\omega_\alpha = \sqrt{k_\alpha / J_\alpha} = \{0.3, 0.4, 0.5\}$ [rad/s] (i.e., three scenarios). If the stabilizers are installed at deck sections $x_{\Omega,1} = 0.25\ell$ and $x_{\Omega,2} = 0.75\ell$, we note that the torsional modal rotations of $v1$ are $\theta_{t1}(x_{\Omega,2}) = -\theta_{t1}(x_{\Omega,1})$, since this bridge has fundamental skew symmetric deck modes. Consequently, the sign of the gyricity Ω, i.e., angular velocity ω_G imparted to the device, installed at $x_{\Omega,2}$, must be appropriate to avoid counteracting the effects of the device at $x_{\Omega,1}$, and reducing the compound gyroscopic effect.

4. CONCLUSIONS AND OUTLOOK

The investigation conducted on the benchmark bridge model for different values of gyricity confirmed the beneficial effects of the multi-unit device on the structure and a noteworthy increment of critical flutter velocity. The increase of performance against flutter depends on the angular velocity ω_G of the gyroscopic effect and the pulsation ω_α of the stabilizers. Compared to the reference flutter velocity without stabilizers (19.75 m/s) Jain (1996), the flutter threshold doubles (increment of 100%) if gyroscopes with angular velocity $\omega_G = 100$ rad/s are installed. Research is still ongoing to optimize the performance for other configurations and long-span bridges. Studies will also investigate the behaviour of the gyroscopic devices, accounting for the eccentricity of the lumped mass $M_{G,TOT}$, design imperfections and installation misalignments.

REFERENCES

Carta, G., Jones, I.S., Movchan, N.V., Movchan, A.B. and Nieves, M.J., 2017. Gyro-elastic beams for the vibration reduction of long flexural systems. Proceedings of the Royal Society A: Mathematical, Physical and Engineering Sciences 473, 1-17.

Chen, X. and Kareem, A., 2003. Efficacy of tuned mass dampers for bridge flutter control. Journal of Structural Engineering, ASCE 129, 1291-1300.

D'Eleuterio, G.M.T., 1986. Dynamics of gyroelastic vehicles. Institute for aerospace studies, Toronto.

Ghommema, M., Nayfeh , A.H., Choura, S., Najar, F. and Abdel-Rahman, E.M., 2010. Modeling and performance study of a beam micro gyroscope. Journal of Sound and Vibration 329, 4970-4979.

Giaccu, G.F. and Caracoglia, L., 2021. A gyroscopic stabilizer to improve flutter performance of long-span cable-supported bridges. Engineering Structures 240, 112373.

Jain, A., 1996. Multi-mode aeroelastic and aerodynamic analysis of long-span bridges. PhD Dissertation, Johns Hopkins University, Baltimore, Maryland, USA.

Kan, Y., Psinh, Y. and Lee, A.-C., 1992. Investigation on the steady-state response of a symmetric rotors. Journal of Vibration and acoustics 114.

Kobayashi, H. and Nagaoka, H., 1992. Active control of flutter of a suspension bridge. Journal of Wind Engineering and Industrial Aerodynamics 41, 143-151.

Kwon, S.-D. and Chang, S.-P., 2000. Suppression of flutter and gust response of bridges using actively controlled edge surfaces. Journal of Wind Engineering and Industrial Aerodynamics 88, 263-281.

Kwon, S.-D., Sungmoon Jung, M.S. and Chang, S.-P., 2000. A new passive aerodynamic control method for bridge flutter. Journal of Wind Engineering and Industrial Aerodynamics 86, 187-202.

Omenzetter, P., Wilde, K. and Fujino, Y., 2002. Study of passive deck-flaps flutter control system on full bridge model. Part 1: Theory. Journal of Engineering Mechanics 128, 264-279.

Pourzeynali, S. and Datta, T.K., 2003. Fatigue reliability analysis of suspension bridges due to gustiness of wind. Proceedings of Int. Conference "Response of Structures to Extreme Loading 2003", Toronto, Canada, CD-ROM.

Scanlan, R.H. and Tomko, J.J., 1971. Airfoil and bridge deck flutter derivatives. Journal of Engineering Mechanics, ASCE 97, 1717-1737.

Wilde, K., Omenzetter, P. and Fujino, Y., 2001. Suppression of bridge flutter by active deck-flaps control system. Journal of Engineering Mechanics 127, 80-89.